Silicon (2024) 16:1881–1892
https://doi.org/10.1007/s12633-023-02819-3

RESEARCH

Preparation and Characterization of Nano Glass–ceramics from CeO_2-doped Li_2O-SiO_2 System for Dental Applications

M. A. Marzouk[1] · H. A. Elbatal[1] · F. H. Elbatal[1] · M. A. Azooz[1] · R. L. Elwan[1] · A. M. Fayad[1] · M. A. Ouis[1] · A. Kh. Helmy[1] · Y. M. Hamdy[2]

Received: 18 October 2023 / Accepted: 13 December 2023 / Published online: 27 December 2023

Abstract
Glasses based on the basic composition of lithium disilicate ($Li_2O.2SiO_2$) together with derived samples containing increasing CeO_2 replacing Li_2O (0.1, 0.2, 0.5, 1 Mol %) were prepared by melting – annealing method, samples from the prepared parent glasses were thermally heat treated through two-step regime (450° C /10 h – followed by 650° C / 6 h) to convert them to their glass – ceramics derivatives. The main purpose of this study is to find out the main properties of the prepared glass – ceramics to be applied as dental candidates. The optical, FTIR, and thermal expansion properties of the parent glasses were examined to identify the main structural groups which are defined as tetrahedral stronger SiO_2 building groups. The detailed separated crystalline phases within the prepared glass–ceramics were identified together with their textural features. The Vickers microhardness data for both the parent glasses and their glass -ceramics derivatives were evaluated. SEM and EDAX measurements indicate the ability of the prepared samples to form hydroxyapatite upon immersion in SBF solution.

Keywords Lithium · Silicate · Glass · Nano · Glass –Ceramics · Dental

1 Introduction

During the past years, numerous scientists have been interested in scientific research on various glass–ceramics suitable for dental applications [1–10]. The importance of glass–ceramics candidates comes from their development by controlled crystallization of specified and selected parent glasses with various forms and textures and hence form an important group of biomaterials used in modern dentistry.

These dental glass–ceramics should possess exceptional aesthetics, translucency, high strength, favorable chemical durability, wear resistance, biocompatibility, low thermal conductivity, and similar or very close microhardness values to that of natural teeth. The choice of these materials comes from the concept that they are easy to prepare with variable shapes to produce the parent glasses and with the proper thermal heat-treatment complete the final formation of glass–ceramics with desirable properties. It is recognized that [6] among the most promising materials, selected glass–ceramics, zirconia (ZrO_2) hybrids, and glass-infiltered ceramics are considered of great importance in these applications [6–11].

Previous publications [5, 6, 11–17] have categorized dental ceramics into three groups: (i) glass-matrix ceramics, (ii) polycrystalline ceramics, and (iii) resin-matrix ceramics. It seems that the best classification of dental glass–ceramics which needs to be mentioned is referred to bioactive type and restorative type. The first bioactive type of glass–ceramics are materials that show bone (teeth) bending ability and also stimulate a particular biological reaction at the interface. In particular, most restorative dental glass–ceramics are inert and biocompatible and generally be used in the restoration and reconstruction of teeth [10–12].

Some authors[1, 7] have referred that many glass–ceramics that can be recommended for dental applications comprise some silicate-heated candidates such as mica-based glass–ceramics, leucite-based glass–ceramic, and lithium disilicate glass–ceramics.

✉ M. A. Marzouk
Marzouk_nrc@yahoo.com

[1] Glass Research Department, National Research Centre, 33 EL Bohouth St. (Former EL Tahrir St.), P.O.12622, Dokki Giza, Egypt

[2] Spectroscopy Department, National Research Centre, 33 El Bohouth Street (Former EL Tahrir), P.O. 12622, Dokki, Giza, Egypt

Hassan and Gad [13] have made a study to compare or rank the wear performance of three different ceramic systems (monolith zirconia, lithium disilicate glass–ceramic and feldspathic porcelain) and their effects on the wear and surface roughness of their antagonist enamel. The conclusion was reached that monolith zirconia and porcelain resulted in less wear to human enamel compared to lithium disilicate-based glass–ceramics. However, porcelain is more affected by wear compared to zirconia.

Several scientists for restorative dentistry have compared three ceramic materials for digital dentistry [14]. The selected materials include fit of metal, lithium disilicate, and zirconia crowns.

The appealing features of certain types of lithium disilicate glass–ceramic warrant further investigation as bioactive dental materials. These substances have been proposed for application in implant coating, bone regeneration, hypersensitivity therapy, periodontal healing, and bone/tooth bonding. They also exhibit the capacity to induce a specific biological response at the material/tissue interface. The characteristics and requirements of the materials used in dentistry have been outlined in several international standards. For example, a dental material needs to have very good mechanical, chemical, and optical qualities that are similar to those of real teeth. On the other hand, in order to improve mechanical qualities including hardness, elastic modulus, brittleness index, chemical solubility, and increased machinability, the parent glass or ceramics may need to have some stabilizers added. CeO_2 can operate as a nucleating agent in the glass ceramic matrix, as stated by earlier studies, and it can induce a characteristic alteration in the crystal morphology of the generated phases, which in turn has a characteristic effect on the crystallite size. Additionally, the inclusion of CeO_2 increased the material's strength, microhardness, and yellow colors, making it a viable option for denture replacement materials [18, 19].

The present study aims to prepare parent glasses based on the Li_2O-SiO_2 system with samples containing added dopant (0.1, 0.2, 0.5, or 1%) percent of CeO_2. The parent glasses were primarily characterized for their optical, FTIR spectral analysis beside thermal expansion measurements. Samples from the glasses were thermally heat-treated to convert them to their corresponding glass–ceramic derivatives through two step regime based on derived data from DTA and thermal expansion parameters.

The derived glass–ceramics were specifically characterized by investigation by FTIR, X-ray diffraction and SEM measurements. These collective analysis are expected to identify the crystalline phases formed by thermal heat-treatment and their morphological textures. Also, the role of the CeO_2 on the chemical and Vickers microhardness data will be evaluated to justify their mechanical properties and suitability to dental applications.

2 Experimental Details

2.1 Preparation of the Parent Glasses

The parent glasses were synthesized from chemicals with a purity of 99.9% (Sigma Aldrich Company). Lithium carbonate (Li_2CO_3) is used as a source of Li_2O while silica (SiO_2) and CeO_2 were used as such. The detailed chemical compositions of the prepared glasses are listed in Table 1. The weighed batches were melted into platinum crucibles at 1400°C and the melting was extended to 2 h with frequent rotating the crucibles at intervals to reach complete mixing and homogeneity. Then the finished melts were poured into warmed stainless steel molds. The prepared glassy samples were transferred immediately into a muffle furnace adjusted at 400°C. After 1 h, the annealing muffle was switched off and left to cool to room temperature with the heated glass samples inside.

2.2 Preparation of the Glass–ceramic Derivatives

The parent glasses were subjected to a controlled thermal heat-treatment process to convert them to their corresponding glass ceramics derivatives using a two-step regime.

The glasses were first heat treated slowly (5°C/ min) to the first selected temperature (450°C) derived from thermal expansion data and previous DTA of the base glass. The temperature was kept at this temperature for 10 h. Then the muffle was raised to the second selected temperature at (650°C) and the temperature was fixed for another 6 h. After that, the muffle was shut down with the heat-treated samples inside and left to cool to room temperature.

The two main steps of crystallization were selected for obtaining a desired homogenous crystal with an acceptable particle size. In the two-step crystallization, the lower temperature allows the crystallization process to begin from the surface, then reformed to become a part of the crystal while the crystal growth is developed and dispersed homogenously toward the bulk body of sample with a fixed rate. This process is used in the majority of silicate-based glasses, which

Table 1 Chemical composition of the prepared undoped and CeO_2 – doped lithium silicate glasses

Sample code	Composition in Mol%		
	SiO_2	Li_2O	CeO_2
S1	68	32	0
S2	68	31.9	0.1
S3	68	31.8	0.2
S4	68	31.5	0.5
S5	68	31	1

may lead to the required microstructure that reflecting on the final glass–ceramic qualities.

2.3 Characterizations Measurements for Properties of Glass–ceramic Derivatives

The derived glass–ceramic were characterized by measuring their FTIR and X-ray diffraction to identify the component structural groups and the type of crystalline phases formed by thermal heat treatment and followed by SEM to specify the structural formations and textures in the background. The X-ray apparatus is a diffractometer (type Philips PW 1390) adopting Ni-filter and Cu-target. The SEM apparatus used was model Philips XL 30. All studied samples were coated with a surface layer of gold to clarify the texture differences. Additionally, a high-resolution transmission electron microscope (TEM, JEOL TEM-2100) was employed to evaluate the produced glasses' morphological characteristics.

In order to estimate the bioactivity, the glass and their corresponding glass–ceramic specimens were soaked in a cellular simulated body fluid (SBF, 50 mL) with ion concentrations and a pH that was almost identical to those of human blood plasma. Reagent grade NaCl, $NaHCO_3$, KCl, K_2HPO_4-$3H_2O$, $MgCl_2$-$6H_2O$, $CaCl_2$, and Na_2SO_4 were dissolved in ion-exchanged water inside a polystyrene bottle to create the SBF, in accordance with Kokubo [20]. In the previous specified order, these reagents were added. The solution was held at ± 37°C and its pH value was adjusted to ≈7.25 using 50 mM Tris-(hydroxymethyl)-amino methane (also known as (CH2OH)3CNH2)) and 45 mM hydrogen chloride. The soaking process was conducted for four weeks at 37°C with constant stirring.

2.4 Measurements of Physical Properties for Parent Glasses

The parent glasses were examined for their optical and FTIR absorption spectra beside their thermal expansion properties.

The thermal expansion behaviors of the parent glasses were measured by a computerized dilatometer(type NETZCH-Dil-402, Germany). All measurements were carried out from room temperature up to the dilatometric softening temperature of each glass sample with a heating rate of 5°C/min.

Fourier transform infrared absorption spectra were recorded using the KBr disc technique using (Nicolet is 10 S spectrometer, USA) within the range 4000–400 cm^{-1} with a resolution of 2 cm^{-1} at room temperature.

Optical (UV–visible) absorption spectra were measured for polished samples of equal thickness (2 mm ± 0.1 mm) within the range of 200–1100 nm using a recording spectrophotometer (type Jasco 630, Japan).

Vickers microhardness data were collected by measuring polished samples through indentations by a Microhardness apparatus (Type Shimadzu, Japan) with a load of 100 gms for 15 s in 5 different places.

3 Results and Discussions

3.1 Differential Thermal Analysis (DTA) and Thermal Expansion Data

Figure 1 shows the DTA of lithium-silicate glasses with 0 mol%, 0.5 mol%, and 1 mol% CeO_2 in the temperature range 200–900 °C with the heating rate of 5° C / min. a characteristic exothermic peak can be observed around 650 °C, and T_g is showing to increase from about 442 °C to 472 °C with increasing CeO_2 content. Such thermal behavior reveals that CeO_2 concentration plays an important role

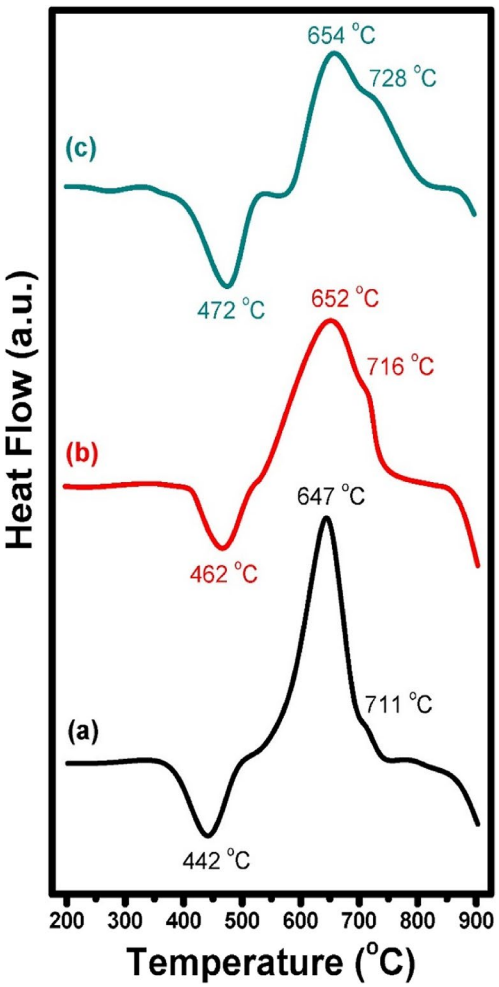

Fig. 1 Differential thermal analysis of the prepared undoped and CeO_2—doped lithium silicate glasses with 0(**a**), 0.5(**b**), and 1 (**c**) mol% CeO_2

in the crystallization behavior of lithium silicate glasses. The possible existence of CeO_2 in the glass network forming position allows the network structure to become more compact which raises the exothermic temperature [21]. In accordance with DTA results obtained in Fig. 1, a heat treatment program was used to produce glass–ceramic derivatives by heating the undoped sample and CeO_2 – doped lithium silicate glasses to 450 °C for 10 h followed by 650°C for 6 h at a rate of 5°C/min. On the other hand, the derived thermal expansion curves of the undoped and CeO_2 – doped lithium silicate glasses are shown in Fig. 2. The measured parameters of dilatometric softening temperature and thermal expansion coefficient (CTE) of the parent glass is shown to progressively increase with the increase of CeO_2 dopant percent up to 0.5% while CTE value is declined with 1% CeO_2 content. In this study, the glass transformation temperature, dilatometric softening temperature and thermal expansion coefficient are 403–494 °C, 434–551 °C, 6×10^{-6} °C – 11.1×10^{-6} °C, respectively.

In most cases, heating is assumed to cause glasses to expand like normal solids. The type of glass, its chemical composition, bond strength, and field strength of the cations are only of the variables that affect the thermal expansion coefficient, glass transformation temperature, and dilatometric softening temperature of glasses [22, 23].

The presence of nonbridging oxygens is highly potent when evaluating the thermal expansion data. The variation of the coefficient of thermal expansion (CTE) and glass transformation temperature with mol% of cerium oxide can be attributed to the progressive formation of non-bridging oxygens (NBSs) which should exhibit a higher value of CTE [24]. Regular expansion is defined as the reaction to the increase of the amplitude-increased atomic vibrations of the constituents during heating, hence the sudden reduction of the dilatometric softening temperature could be attributed to be due to the reduction of the stress arising in glass upon quenching or rapid cooling during synthesis or rapid annealing [25, 26]

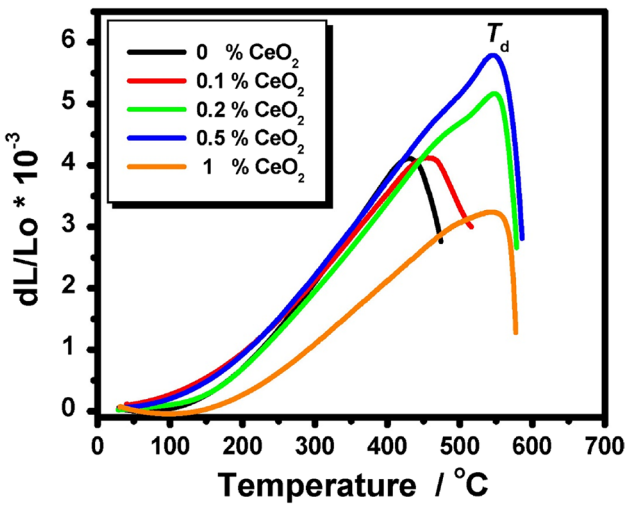

Fig. 2 Thermal expansion of the undoped and CeO_2 – lithium silicate glasses

3.2 X-ray Diffraction Patterns of the Heat-treated Glass – ceramic Derivatives

The derived x-ray diffraction patterns of the heat-treated undoped and CeO_2—doped lithium silicate glasses are shown in Fig. 3. The undoped and 0.1mol % CeO_2 glass–ceramics (Fig. 3a and b) exhibit similar peak positions and reveal two characteristic crystallite phases that are correlated to $Li_2Si_2O_5$ and Li_2SiO_3 crystalline phases that corresponded to PDF cards No. 40–0376 and 15–0519, respectively. The progressive increase of CeO_2 concentration up to 1% leads to a newly induced diffraction pattern

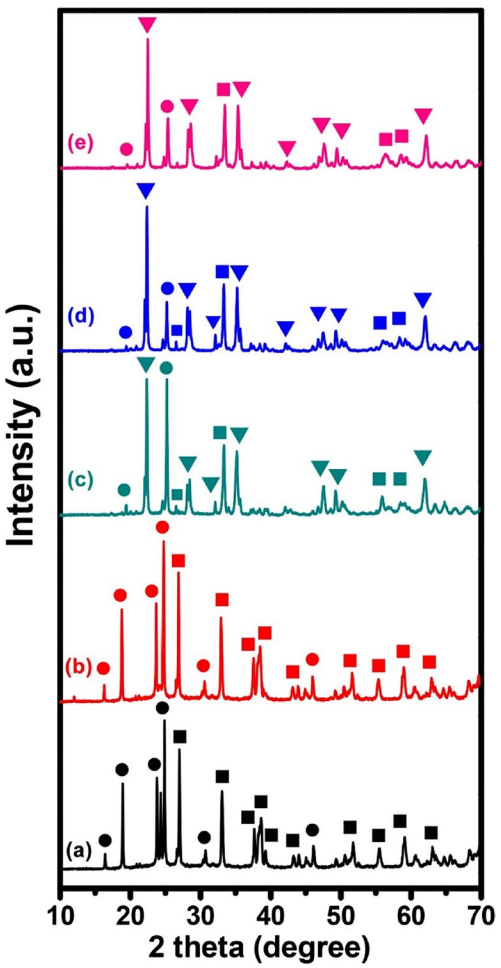

Fig. 3 XRD of the heat–treated glasses where (**a**) undoped, (**b**) 0.1 % CeO_2 , (**c**) 0.2 % CeO_2 , (**d**) 0.5 CeO_2 and (**e**) 1 % CeO_2 while the crystallite formed phases denoted as ●=$Li_2Si_2O_5$, ■=Li_2SiO_3, and ▼=Li_4SiO_4

correlated to Li_4SiO_4 that matched with PDF No. 700–2340. It is clear that CeO_2 did not form a separate crystalline phase in the parent glass due to its presence within the constituent network units, but rather acted as a catalyst to accelerate the crystallization process. According to reports and publications [27–29], CeO_2 is a network modifier that easily breaks silicon-oxygen bonds and creates more crystal defects, which is advantageous for the nucleation and transformation of lithium silicate matrix.

The realization and explanations of the mode for crystallization behavior are based on the following basis [27–29]:

(i) The presence of a sufficient percent of Li_2O in the composition of the glasses promotes ease of nucleation, phase separation, and subsequent full crystallization, and hence the lithium ions are considered to be self–nucleating ions. The identification of two crystalline phases from lithium silicates is familiar and expected beside the appearance of excess silica which separates as symmetrical quartz.

(ii) The doping of the parent glass with varying CeO_2 percents is observed to cause variable changes in the formed crystalline phases. At low percent, the lithium aluminum silicate phases are the dominant, and aluminum ions are derived from the presence of nano silica used for the preparation of the glasses which do contain Al_2O_3 (0.44), CaO (0.03), ZrO_2 (0.01), L.O.I (3.24). it is assumed that the CeO_2 acts at first as a nucleator or promotor to the crystallization process and also shares in the separation of crystalline (CeO_2). At a high percent, the role of CeO_2 is only as a promotor (or nucleator) to enhance the formation of three types of LiAl silicate and symmetric quartz.

3.3 TEM, SEM and EDX Measurements

Figure 4 represents the TEM of the selected 0.1 and 1 mol% CeO_2 samples. TEM Figure shows evidence of the crystallization of one or more phases. Also, In the quenched 0.1 and 1 mol % CeO_2 samples, TEM exhibited precipitation of nano-sized crystals of just the lithium silicate phase as illustrated by the XRD analysis. The TEM figure is a confirmation of the formation of many crystalline nano-phases phases around 25–30 nm for 0.1 mol % co-doped sample and 10–12 nm for 1% CeO_2 co-doped sample. The crystal size was decreased by increasing the CeO_2 content.

Figures 5, 6, 7 and 8 depict the EDAX analysis and SEM morphology of CeO_2 doped glass and glass–ceramic samples after immersion in the simulated body fluid solution for 4 weeks which indicates the elemental growth of P and Ca. EDAX results show sharp intensity peaks for Ca and P which are more pronounced in the glass–ceramics derivative than their glass. The micrographs of both glasses and glass–ceramic samples reveal some microcrystalline texture with rounded small crystals dispersed on the surface. When lithium silicate glass or glass–ceramic is immersed in SBF, the net result that a polycondensation reaction is assumed to lead to the formation of the silanol groups, which causes calcium ions to react with phosphate ions to form a mixture of calcium phosphate, and ultimately causes the formation and growth of calcium phosphate, which will crystallize to surface as hydroxyapatite (HAP) [30].

3.4 FT Infrared Spectra of the Parent Glasses

Figures 9, 10 and 11 show the FTIR spectral curves of the parent glasses. The identified vibrational bands are observed to extend from 400 to 1700 cm^{-1} and end with a broad near IR band extending from about 2000 cm^{-1}. The detailed IR spectral absorption shows small far-IR peaks extending from 400–520 cm^{-1} followed by a medium band with two peaks at 630 and 670 cm^{-1} and succeeded by two broad bands, the first extends from about 720 to 1100 cm^{-1} with three small peaks about 880, 950 and 1050 cm^{-1} and the second band reveals sharp peak at 1385 cm^{-1}, which is followed by an attached peak at the descending lobe at 1619 cm^{-1}.

Figure 11 reveals the FTIR of the corresponding glass–ceramic derivatives.

Inspection the IR curves of glass -ceramics shows almost similar IR spectra to that obtained from their parent glasses.

The explanation and interpretations of the resultant identified IR spectra are based on the following [31–35]:

(i)It is accepted that the identified IR vibrational bands collected from glasses are correlated with the vibrations of existing structural groups or units within the network of the examined glasses depending on chemical constituents.

(ii) The detailed chemical composition of the glass and the expected structural units from them are the source of the IR absorption bands.

(iii) The basic or fundamental building units in the studied lithium silicate glasses are tetrahedral SiO_4 units in which all oxygens are shared between two tetrahedra, forming a fully polymerized units. The introduction of alkali oxides as fluxes causes the formation of nonbridging oxygens and the alkali cations (Li^+) are situated in interstitial sites to the tetrahedral network and in the vicinity of the negatively charged nonbridging oxygens (NBOs).

(iv) Based on previous publications on IR spectra of silicate glasses, the following assignments are introduced for the collected data [31–37]:

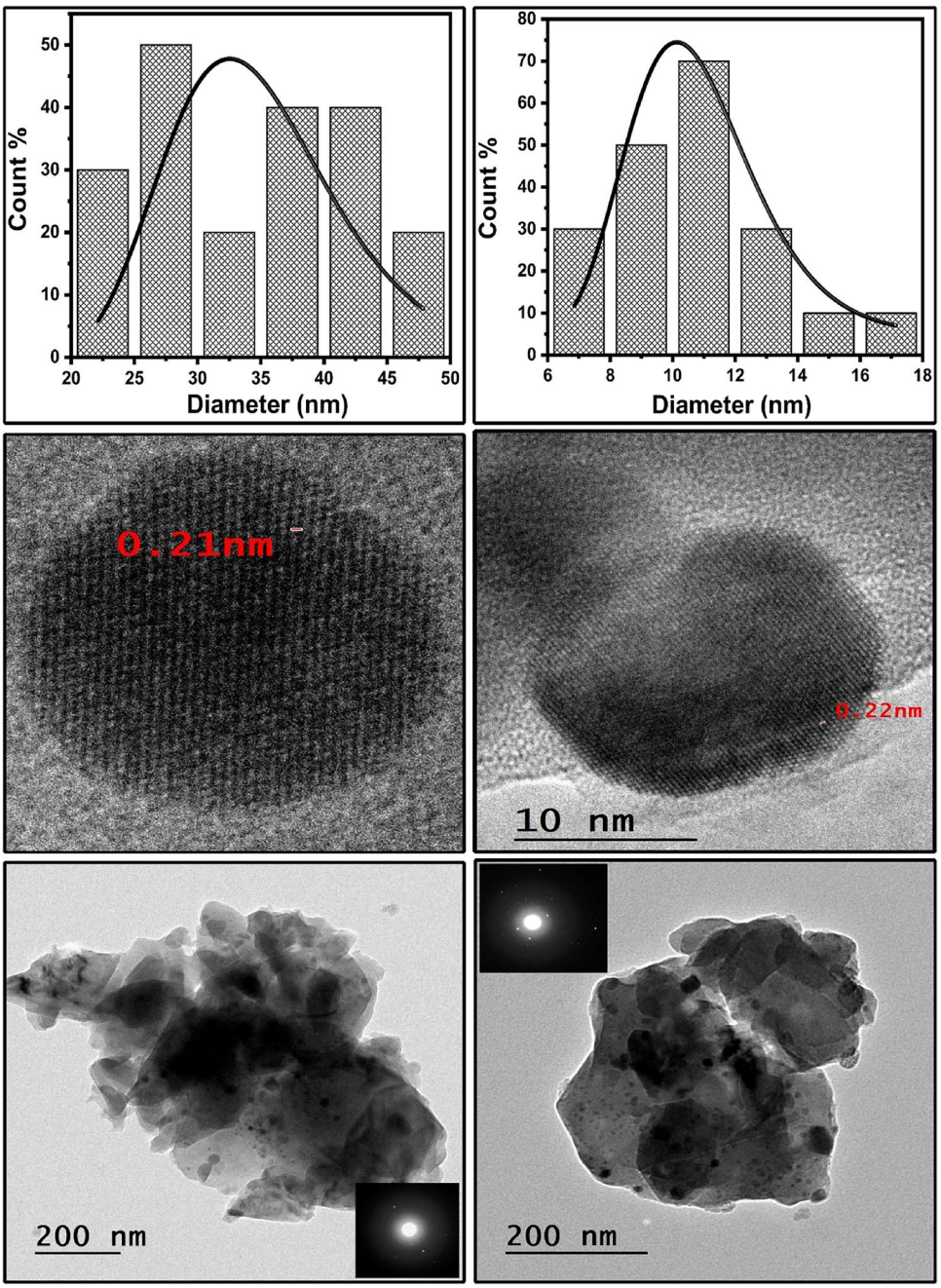

Fig. 4 TEM of the heat-treated glasses and their particle size distribution histogram where the left side corresponds to $0.1CeO_2$ and the right side for 1% CeO_2 samples

(a) The identified far IR peaks within the range 400–480 $cm^{-1}$are correlated with vibrations of Li^+ cations within their characteristic sites.
(b) The vibrational peaks within the region 580–650 cm^{-1} are related to bending modes of Si–O-Si or O-Si–O bonding
(c) The IR bands within the range 720–800 cm^{-1} are attributed to Si–O-Si symmetric stretching vibrations.
(d) The IR bands within the range 950–1100 cm^{-1} are related to Si–O-Si antisymmetric stretching vibrations.
(e) The IR bands within the region 1600–1650 cm^{-1} are related to vibrations of OH, water, silanol (SiOH).
(f) FTIR absorption bands of inverted glass samples reveal $Li_2Si_2O_5$ and Li_2SiO_3 phases that can be distinguished by broader bands shape than those

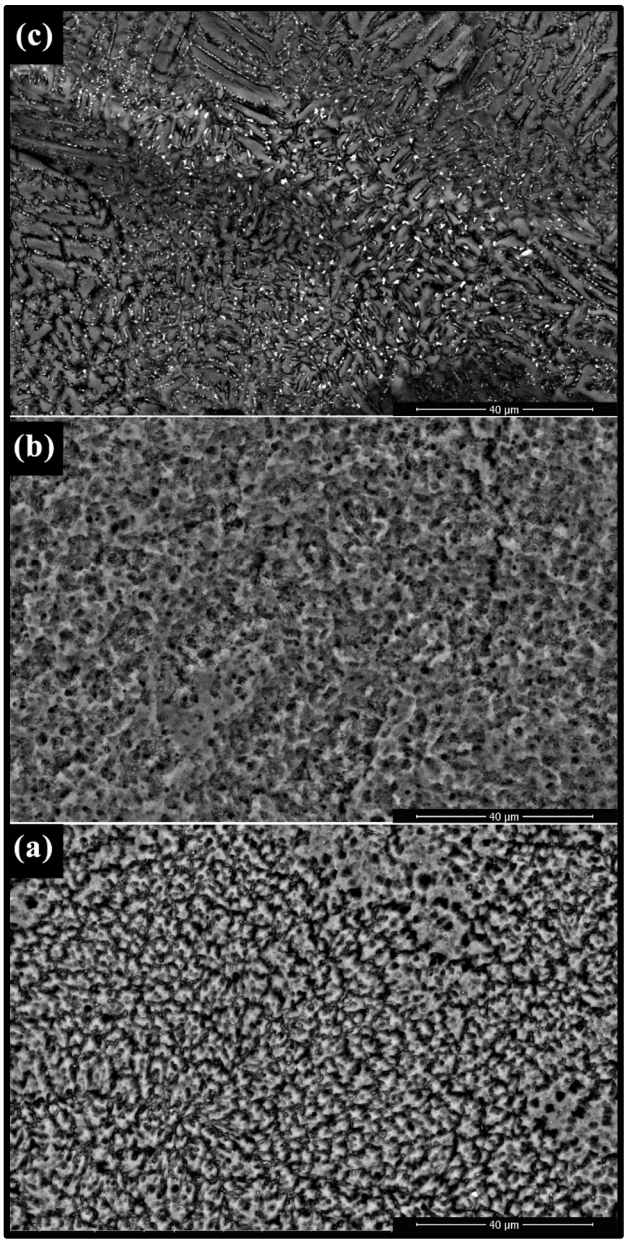

Fig. 5 SEM images of the prepared glass ceramics before immersion where (**a**) 0% CeO_2, (**b**) 0.5% CeO_2 and (**c**) 1% CeO_2

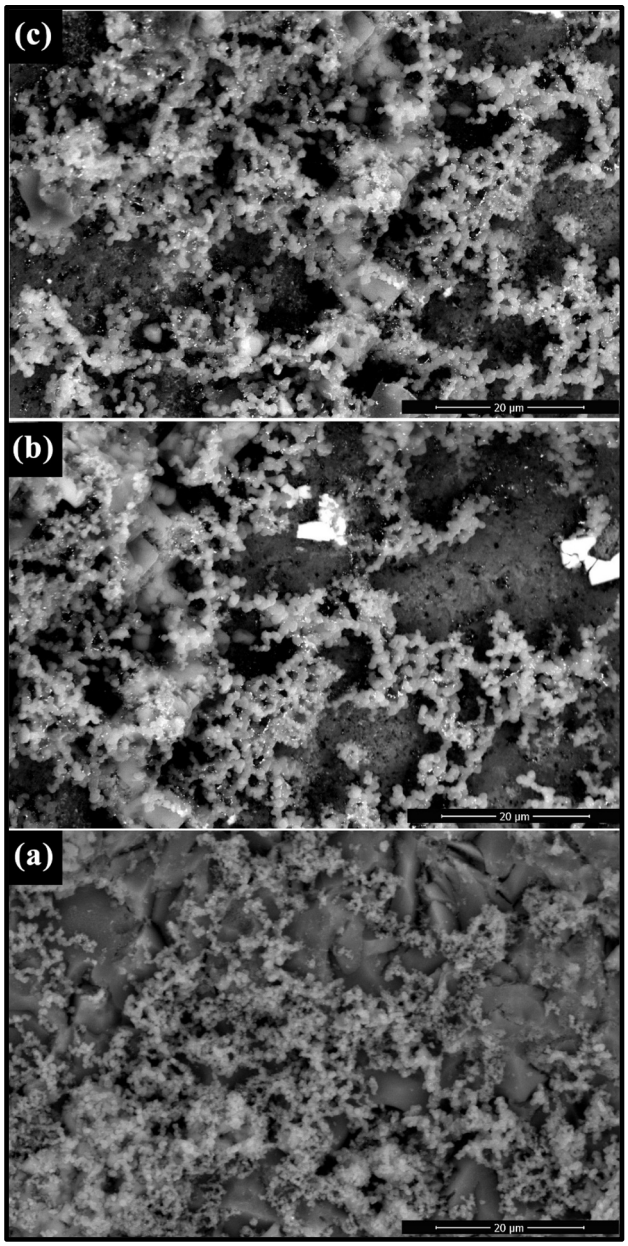

Fig. 6 Figure 3 SEM of the prepared glass ceramics after immersion 4 weeks in SBF solution where (**a**) 0% CeO_2, (**b**) 0.5% CeO_2 and (**c**) 1% CeO_2

obtained from the glassy matrix or coexist with additional sharp bands. The characteristic Si–O stretching modes in crystalline Li metasilicate, Li_2SiO_3, and Li disilicate, $Li_2Si_2O_5$, where the silicate tetrahedra have two (Q^2) and three (Q^3) bridging oxygen ions, respectively, have been measured at 921 and 1023 cm^{-1}.

With reference to the presumptions made earlier [35–37], the term "Q^n structure" refers to the primary structural framework of silicon bond arrangements of tetrahedral form to the nearby oxygen, where n = 0—4 based on the number of BOs. As demonstrated by the thorough deconvolution of the IR spectra shown in Fig. 9, the addition of network modifiers, such as lithium, significantly alters the Q^n structure and subsequently adds new bands to the FTIR spectrum. The silicon network changes to a more chainlike structure when lithium dioxide is added to fused silica. It is in fact implied that the oxygen ions involved are covalently bonded to the silicon ions at one end by the ionic character of the Li–O and Ce–O bonds. Known as "non-bridging oxygens" (NBOs),

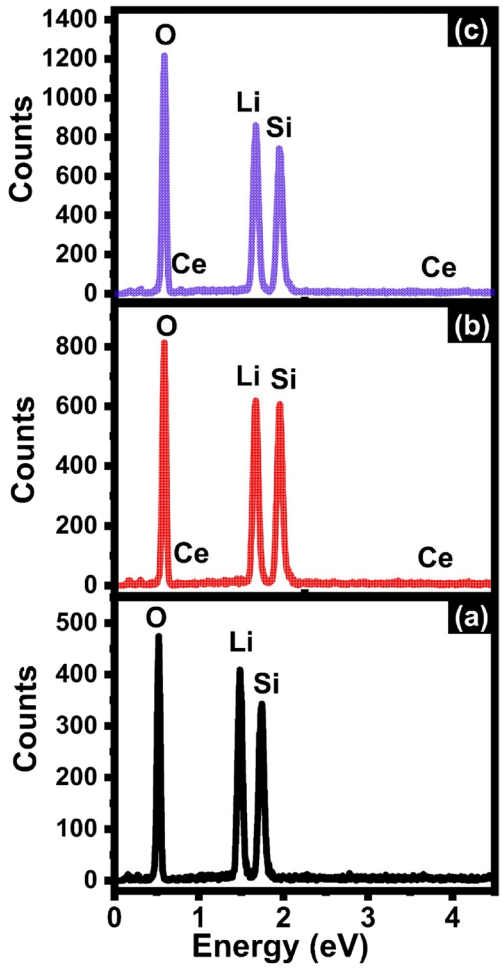

Fig. 7 EDAX analysis before immersion in SBF solution where (**a**) 0% CeO_2, (**b**) 0.5% CeO_2 and (**c**) 1% CeO_2

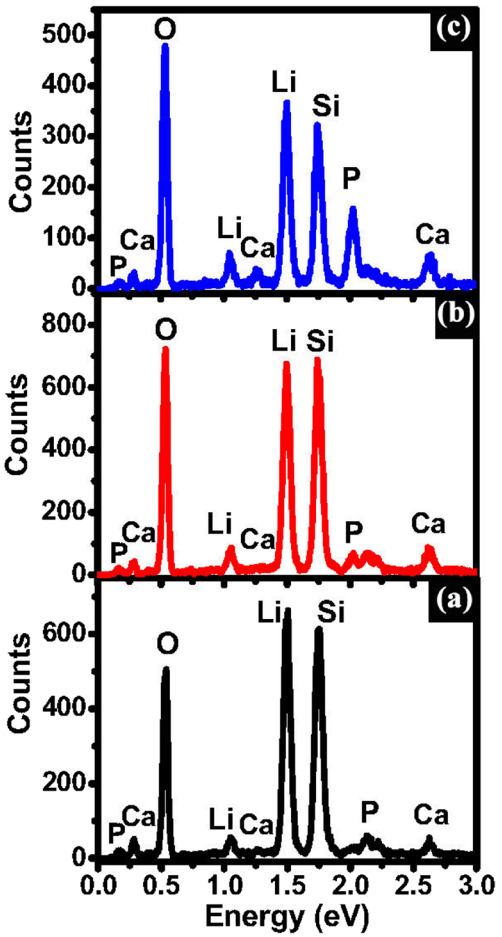

Fig. 8 EDAX analysis after immersion in SBF solution for 4 weeks where (**a**) 0% CeO_2, (**b**) 0.5% CeO_2 and (**c**) 1% CeO_2

these oxygen ions change the three-dimensional silicon network into a silicon structure that is more akin to a chain. The characteristics of glass change as a result of the NBOs' presence, which also causes a decrease in connectivity within the glass network. Specifically, glass transformation temperature (T_g), thermal expansion coefficient, crystallization degree, bioactivity, and optical characteristics.

3.5 UV–visible Absorption Spectra

Figure 12 introduces the absorption and transmission spectra of the base undoped together with that for CeO_2 – doped lithium silicate glasses. The optical spectrum of the undoped sample reveals a distinct UV absorption peak at 364 nm and without any further absorption to the end of measurements. According to Duffy [38] and Ehrt et al. [39, 40], agreed that the recently identified particular UV absorption bands in the various undoped glass samples are considered to be the result of the presence of trace iron ions present as chemical impurities in the chemicals used for the preparation. The optical spectra of CeO_2-doped glasses exhibit extended near-visible absorption to about 450 nm and the spectral curve extended to the longer wavelength with increasing the CeO_2 concentration. The recorded optical transmittance in the UV–VIS region shows a characteristic decrease in the transmission when the dopant amount of CeO_2 is increased up to 1 mol% as represented in Fig. (12b). Furthermore, a cutoff wavelength can be observed depending on glass composition and falling at about 326, 390, 404, 423, and 436 nm, for 0, 0.1, 0.2, 0.5, and 1 mol% CeO_2 respectively.

Cerium ions are assumed to have the ability to exist in two possible valence states in glass, Ce^{3+} and Ce^{4+} with the electronic configuration of f^4 and f^0, respectively and their ratios depend on the host material as well as on the preparation condition [41]. The optical absorption spectrum of Ce^{3+} ions is an allowed transition ($f^4 \rightarrow d^1$) which depends strongly on the host materials, but very often appears in the UV range in most of the oxide glasses [42]. The identified characteristic optical absorption spectra could be attributed

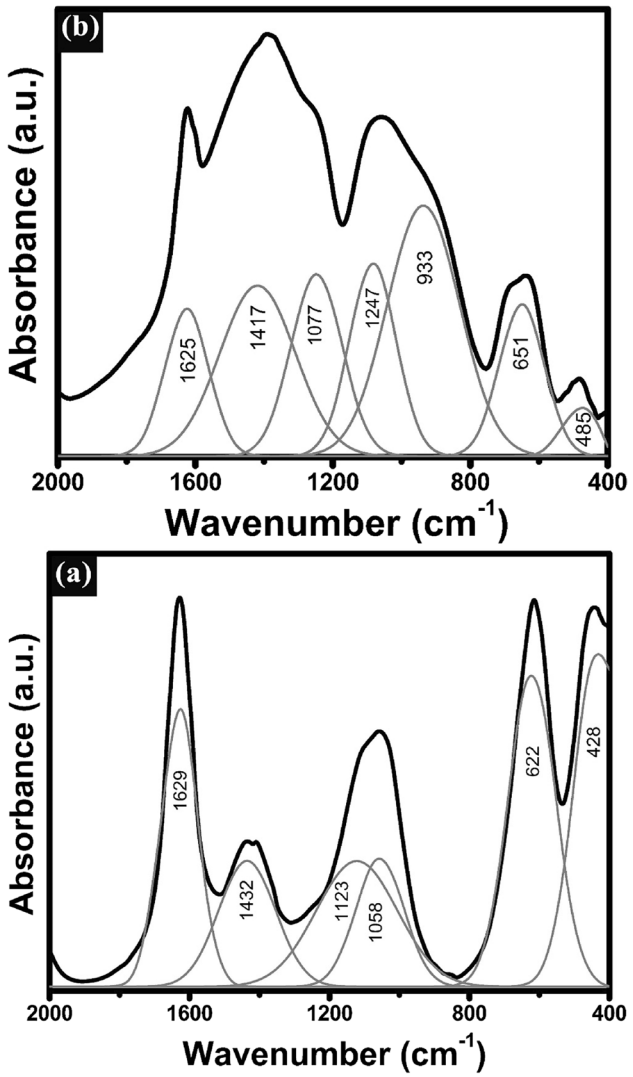

Fig. 9 FTIR of the base undoped glass where (**a**) glass and (**b**) glass – ceramics

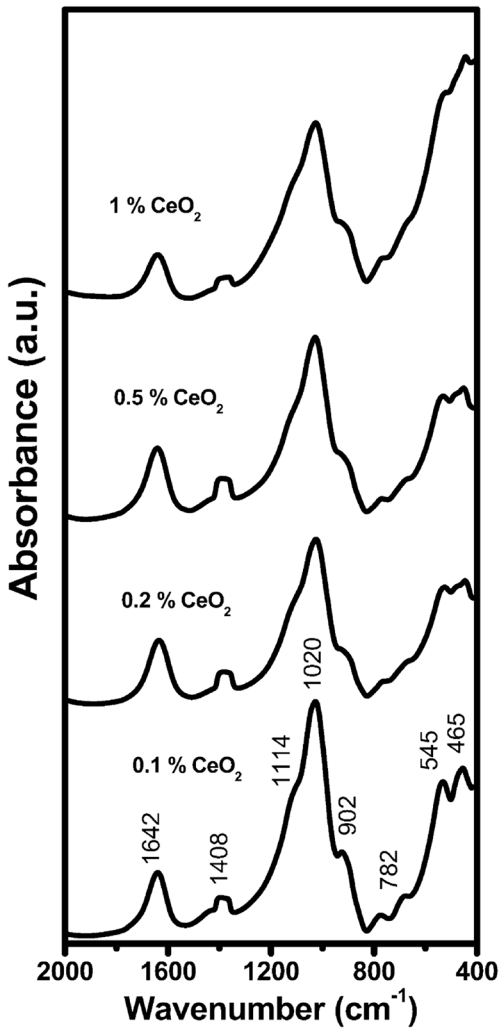

Fig. 10 FTIR of CeO_2 – doped glasses

to the characteristic peak of Ce^{3+} which generates a yellowish appearance [40, 42].

3.6 Microhardness Measurements

It is realized that during the Vickers microhardness measurements, the diamond indenter produces noticeable indentation within the surface of the glass, the depth and dimension of which vary with the type and composition of the measured glass [43–45]. Some different mechanisms have been proposed to explain the way of generation of the indentation, such as plastics or viscous flow or densification [43–45]. The previous studies suggested processes are assumed to be correlated with the percents of both network former ions and also the modifying ions and the bending strength between former and modifier ions. Silicate glasses and glass – ceramics with high SiO_2 contents possess higher values of Vickers microhardness values and Corning Glass Works (USA) recommended some glass -ceramics for aerospace applications.

Table 2 depicts the Vickers microhardness data of the parent glasses and their glass – ceramics derivatives. The results reveal that the microhardness progressively increases with increase of CeO_2 in both the glasses and glass–ceramics. Also, the data show that the glass – ceramics exhibit higher microhardness values than their parent glasses. The collective data indicate that CeO_2 causes compactness in the network structures of all samples leading to the obvious increase in the microhardness values. Also, as expected the glass – ceramics derivatives possess after preparation defined crystalline textures which virtually promotes higher microhardness values.

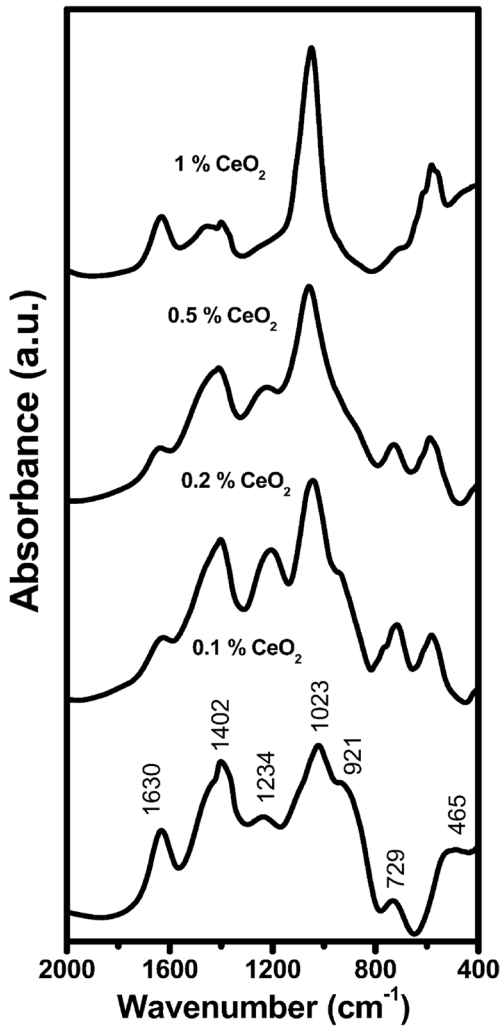

Fig. 11 FTIR of the CeO_2-doped glass – ceramics

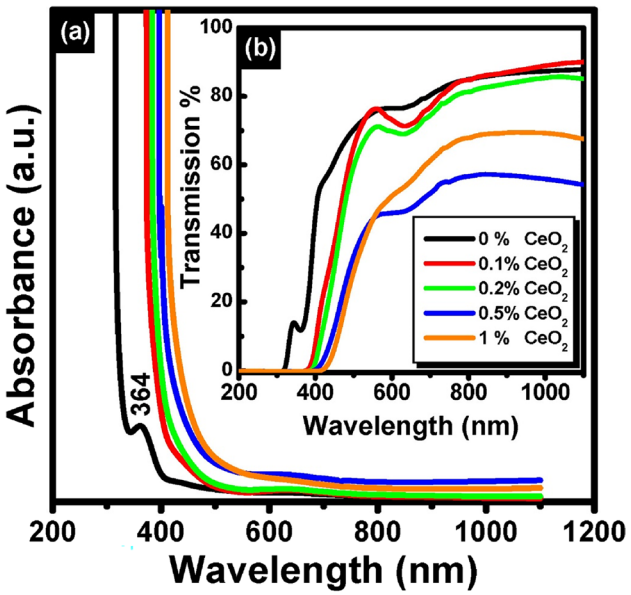

Fig. 12 UV–visible (**a**) absorption and (**b**) Transmission of undoped and CeO_2-doped glasses

Table 2 Microhardness (Kg mm^{-2}) of the prepared glasses and their corresponding glass—ceramics

Sample	Glass	Glass – ceramics
1	443	450
2	453	455
3	459	470
4	472	581
5	490	610

4 Conclusions

Undoped Lithium disilicate glasses with the nominal composition SiO_2 – (32-x) Li_2O – $xCeO_2$ in mol% (where x = 0, 0.1, 0.2, 0.5, and 1) were prepared via conventional melt-quenching method. From the DTA measurements, the samples undergo a controlled heat treatment at 450° C and 650° C for 10 and 6 h respectively to obtain the corresponding glass–ceramics. The dilatometric softening temperature and thermal expansion coefficient (CTE) gradually rise as CeO_2 dopant percent increases up to 0.5%, while the CTE value decreases as CeO_2 content increases to 1%. Two distinct crystallite phases were identified by XRD analysis respectively, and are associated with the $Li_2Si_2O_5$ and Li_2SiO_3 crystalline phases together with a freshly created diffraction pattern of Li_4SiO_4 phase that is produced when the concentration of CeO_2 is gradually increased up to 1%. As the CeO_2 content was increased, the crystal size was reduced, and the TEM figure confirms the production of many crystalline nano-phases approximately 25–30 nm for the 0.1 mol% co-doped sample and 10–12 nm for the 1% CeO_2 co-doped sample. The glass or glass–ceramic reveals a bioactive behavior and the growth of crystallite hydroxyapatite (HAP) on the surface is directly proportional to CeO_2 content. The basic or fundamental building units in the studied lithium silicate glasses are tetrahedral SiO_4 units in which all oxygens are shared between two tetrahedra, forming a fully polymerized Si – O – Si and/or O – Si – O units in the extended IR range from 580 to about 1100 cm^{-1}. The IR range 400–480 cm^{-1} are correlated with vibrations of Li^+ cations within their characteristic sites. FTIR absorption bands of the inverted glass—ceramic samples exhibited a broader band shape than those obtained from the glassy matrix. The optical absorption spectra was characterized at 326, 390, 404, 423, and 436 nm, for 0, 0.1, 0.2, 0.5, and 1 mol% CeO_2 respectively. The optical spectra mainly depend on the valence state of cerium ions electronic configuration. In both glasses and glass–ceramics, the microhardness gradually rises as the

amount of CeO_2 increases. Furthermore, compared to their parent glasses, the glass–ceramics had higher microhardness values due to the compactness action of CeO_2. The tested disilicate glasses and their corresponding glass – ceramics co-doped with CeO_2 are suitable for use in dental and biomedical applications.

Acknowledgements The authors of this study wish to thank the National Research Centre authority for the financial support with project No. 13020218.

Author Contributions M. A. Marzouk, H. A. Elbatal, F. H. Elbatal, M. A. Azooz, R. L. Elwan, A. M. Fayad, M. A. Ouis, A. K. Helmy, and Y. M. Hamdy contributed to executing data analysis, writing manuscript, drawing figures, and manuscript revision.

Funding Open access funding provided by The Science, Technology & Innovation Funding Authority (STDF) in cooperation with The Egyptian Knowledge Bank (EKB). The authors declare no Funds.

Data Availability The authors stated and declared that all data exists and is available.

Declarations

Consent for Publication All authors approved the version of the manuscript to be published.

Competing Interests The authors declare no competing interests.

References

1. Höland W, Rheinbrger V, Apel E, Ritzbrger C, Rothbrust F, Kapput H, Krumeich F, Nesper R (2009) Future perspectives of biomaterials for dental restoration. J Eur Ceram Soc 29:1291–1297
2. ElBatal FH, Azooz MA, Hamdy YM (2009) Preparation and characterization of some multicomponent silicate glasses and their glass–ceramics derivatives for dental applications. Ceram Intern 35:1211–1218
3. Pollington S (2011) Novel Glass-Ceramics for Dental Restorations. J Contemp Dant Pract 12:60–67
4. Johnson A, Sinthuprasirt P, Fathi H, Pollington S (2013) Current glass – ceramics used in dentistry. In: Nandyala SH, Santen JD (eds) Current trends in glass and ceramic materials. Bentham Science Publishers Ud, UK, pp 49–72
5. Montazerian M, Zanotto ED (2016) Bioactive glass-ceramics: processing, properties and applications. J Biomed Mater Res Part A 104A:1231–1244
6. Montazerian M, Zanotta ED (2017) Bioactive and inert dental glass-ceramics. J. Biomed. Mater. Res. Part A 105A:619–639
7. Höland W, Beall GH (2020) Glass-ceramic Technology, 3rd edn. The American Ceramic Society, John Wiley, Sons New Jersey
8. Baino F, Tomaliao M, Tylyaganov D (eds) (2021) Ceramics, glass and glass-ceramics from early manufacturing steps towards modern frontiers. Springer Nature, Switzerland AG
9. Lohbauer U, Belli R (2022) Chemistry and microstructure. In: Dental Ceramics. Springer, Cham. https://doi.org/10.1007/978-3-030-94687-6_2
10. Montazerian M, Buino F, Fiume E, Migneco C, Alaghmandfard A, Sedighi O, DeCeanne AV, Wilkinson CJ, Mairo JC (2023) Glass-ceramics in dentistry: Fundamentals, technologies, experimental techniques, applications, and open issues. Prog Mater Sci 132:101023
11. Baino F, Novajra G, Miguez-Pacheco V, Boccaccini AR, Vitale-Brovarone C (2016) Bioactive glasses: Special applications outside the skeletal system. J. Non-Cryst. Solids 432:15–30
12. Gracis S, Thompson VP, Ferencz H, Silva NR, Bonfante EA (2015) A new classification system for all-ceramic and ceramic-like restorative Materials. Int J Prosthodont 28:227–235
13. Hassan SM, Gad NA (2017) Two-body wear and surface roughness of three different ceramic systems and their enamel antagonist: An invitro study. Al-Azhar Dental Journal 4(4):347–357
14. Al Hamad KQ, AlQuran FA, Aljalam SA, Baba NZ (2019) Comparison of the accuracy of fit of metal, zirconia, and lithium disilicate crowns made from different manufacturing techniques. J Prosthodont 28:497–503. https://doi.org/10.1111/jopr.13029
15. Wong J, Angell CA (1976) Glass Structure by vibrational spectroscopy. Marcel Dekker, NewYork
16. Efimov AM (1999) Vibrational spectra, related properties, and structure of inorganic glasses. J Non-Cryst Solids 235:95
17. Merzbacher CI, White WB (1991) The structure of alkaline earth aluminosilicate glasses as determined by vibrational spectroscopy. J Non-Cryst Solids 130:18
18. Srichumpong T, Pintasiri S, Heness G, Leonelli C, Meechoowas E, Thongpun N, Teanchai C, Suputtamongkol K, Chaysuwan D (2021) The influence of yttria-stabilised zirconia and cerium oxide on the microstructural morphology and properties of a mica glass-ceramic for restorative dental materials. Journal of Asian Ceramic Societies 9(3):926–933
19. Montazerian M, Zanotto ED (2017) Review Article. J. Biomed. Mater. Res. Part A 105A:619–639
20. Kokubo T, Kushitani H, Sakka S, Kitsugi T, Yamamuro T (1990) Solutions able to reproduce in vivo surface-structure changes in bioactive glass–ceramic A-W3. J Biomed Mater Res (A) 24:721–734
21. Marzouk MA, Elkashef IM, Elbatal HA (2019) Luminescent, semiconducting, thermal, and structural performance of Ho^{3+}-doped lithium borate glasses with CaF_2 or MgF_2. Appl Phys A 125:97
22. Holloway DG (1973) the Physical properties of glass. Wykeham, London
23. Rawson H (1980) Properties and applications of glasses, Glass Science & Technology, vol 3. Elsevier, Amsterdam
24. Deshpande VK, Taikar RN (2010) Effect of cerium oxide addition on electrical and physical properties of alkali borosilicate glasses. Mater Sci Eng, B 172:6–8
25. Peuget S, Maugeri EA, Charpentier T, Mendoza C, Moskura M, Fares T, Bouty O, Jégou C (2013) Comparison of radiation and quenching rate effects on the structure of a sodium borosilicate glass. J Non-Cryst Solids 378:201–212
26. Eremyashev VE, Zherebtsov DA, Osipova LM, Brazhnikov MV (2018) Effect of calcium, barium, and strontium on the thermal properties of borosilicate glasses. Glass Ceram 74:345–348
27. Zhao X, Gao C, Li B (2020) Effect of CeO_2 on sintering behavior, crystallization, and properties of CaO-Al_2O_3-SiO_2 glass–ceramics for packages. J Mater Sci: Mater Electron 31:17718–17725

28. Hu AM, Liang KM, Zhou F, Wang GL, Peng F (2005) Phase transformations of Li_2O–Al_2O_3–SiO_2 glasses with CeO_2 addition. Ceram Int 31:11–14
29. Lei Y, He Y, Chen FF, Xu J (2015) Effect of Mineralizers and Reaction Conditions on the Formation of Cristobalite. Interceram Int Ceram Rev 64:214–218
30. Marzouk MA, ElBatal HA (2014) In vitro bioactivity of soda lime borate glasses with substituted SrO in sodium phosphate solution. Processing and Application of Ceramics 8(3):167–177
31. Dunken H, Doremus RH (1987) Short time reactions of a Na_2O-CaO-SiO_2 glass with water and salt solutions. J Non-Cryst Solids 92:61
32. Husung RD, Doremus RH (1990) The infrared transmission spectra of four silicate glasses before and after exposure to water. J. Mater. Res. 5(10):2209
33. AboNaf SM, ElBatal FH, Azooz MA (2003) Characterization of some glasses in the system SiO_2, Na_2O·RO by infrared spectroscopy. Mater Chem Phys 77:846
34. ElBatal FH, Khalil EM, Hamdy YM, Zidan HM, Aziz MS, Abdelghany AM (2010) FTIR spectral analysis of corrosion mechanisms in soda lime silica glasses doped with transition metal oxides. SILICON 2:41–47
35. ElBatal HA, Azooz HA, Saad EA, EzzElDin FM, Amin MS (2018) Corrosion behavior mechanism of borosilicate glasses towards different leaching solutions evaluated by the grain method and FTIR spectral analysis before and after gamma irradiation. Silicon 10:1139–1149
36. Seuthe T, Grehn M, Mermillod-Blondin A, Eichler HJ, Bonse J, Eberstein M (2013) Structural modifications of binary lithium silicate glasses upon femtosecond laser pulse irradiation probed by micro-Raman spectroscopy. Optical Materials Express 3(6):755–764
37. Möncke D, Ehrt R, Palles D, Efthimiopoulos I, Kamitsos EI, Johannes M (2017) A multi technique study of a new lithium disilicate glass-ceramic spray-coated on ZrO_2 substrate for dental restoration. Biomed Glasses 3:41–55
38. Duffy JA (1997) Charge transfer spectra of metal ions in glass. Phys Chem Glasses 38:289–294
39. Ehrt D, Ebeling P, Natura U, UV, (2000) Transmission and radiation-induced defects in phosphate and fluoride–phosphate glasses. J. Non-Cryst. Solids 263 264:240–250
40. Möncke D, Ehrt D (2004) Irradiation induced defects in glasses resulting in the photoionization of polyvalent dopants. Opt Mater 25:425–437
41. Marzouk MA, Ali IS, ElBatal HA (2018) Optical, FT infrared and photoluminescence spectra of CeO_2 – doped Na_2O –ZnO – B_2O_3 host glass and effects of gamma irradiation. J Non-Cryst Solids 485:14–23
42. Marzouk MA, ElBatal HA, Hamdy YM, Ezz-Eldin FM (2019) Collective Optical, FTIR, and Photoluminescence Spectra of CeO_2 and/or Sm_2O_3-Doped Na_2O–ZnO–P_2O_5 Glasses. Int J Opt 2019:1–11. https://doi.org/10.1155/2019/6527327
43. Ghoneim NA, El Batal HA, Nassar AMA (1983) Microhardness and softening point of some alumino-borate glasses as flow dependent properties. J Non-Cryst Solids 55:343–351
44. Ghoneim NA, EL Batal HA, Abbas ARF, Ammar MM, Halawa MM (1981) Microindentation Hardness of Silicate Glasses Containing BaO or ZnO. Bull Am Ceram Soc 60:1289–1292
45. Hamzawy EMA, El Batal HA, Azooz MA, El-Bassyouni GT, El Batal FH (2023) Glasses and Glass-Ceramics from Li_2O-KF-TiO_2-SiO_2 System Doped with SiC. SILICON. https://doi.org/10.1007/s12633-023-02531-2